SYSTEM IDENTIFICATION AND MODELING OF BRIDGE SYSTEMS FOR ASSESSING CURRENT DESIGN PROCEDURES

Y. Arici[1] and K. M. Mosalam[2]

Department of Civil and Environmental Engineering
University of California Berkeley

ABSTRACT

The recorded motions by California Strong Motion Instrumentation Program (CSMIP) for seven different bridge systems are analyzed using parametric and non-parametric system identification methods. The results of these analyses include identification of modal frequencies, mode shapes and damping ratios. An excellent fit of the recorded motion in time domain is obtained using parametric methods. Utilizing the results from the identification study, the paper evaluates commonly used bridge design provisions in California.

INTRODUCTION

Identification of structural systems has been a major tool in the last two decades to verify and determine vibration characteristics. Numerous works have been conducted on building systems. In this paper, no attempt is made to review literature on buildings. Instead, the focus of the following concise literature review is on the identification and evaluation techniques performed on bridge structures.

Prior to 1999, there were 54 instrumented bridges in California, 47 of which were instrumented in the last decade. Complete list of instrumented bridges can be found in Hipley (1998). One of the older extensively instrumented bridges is El Centro Highway 8/Meloland Overpass. Several researchers, e.g. Werner et al. (1987, 1994) and Wilson and Tan (1990) have studied this bridge. Modal properties were determined using single-input/single-output and multi-input/multi-output methods. Levine and Scott (1989) used the ground motion recordings for verification of the bridge foundation model they established. Wilson (1986) used the recordings from San Juan Bautista 156/101 Overpass to evaluate the seismic response. Goel and Chopra (1995) studied Rio Dell-Hwy 101/Painter Street Overpass to estimate stiffness of abutments. McCallen and Romstadt (1994) performed detailed finite element modeling to evaluate the same structure. Saadeghvaziri and Foutch (1989) investigated the effects of vertical earthquake motions on highway bridges using data from Rio Dell-Hwy101/Painter Street Overpass. Safak (1994) used data from this bridge subjected to small earthquakes to predict the larger earthquake response. Fenves and Desroches (1994) evaluated the response of Interstate 5/Route 14 interchange using non-parametric and parametric identification

[1] Doctoral Student
[2] Assistant Professor

techniques. Hayward BART elevated section was studied by Tseng et al. (1992) producing results of coupling effects. Dumbarton Bridge has been studied by Fenves et al. (1992) pointing out the importance of articulations and longitudinal constraints at hinges. Abdel-Ghaffar et al. (1993) estimated the modal properties of Vincent Thomas Suspension Bridge from ambient vibration and Whittier earthquake recordings. Lus et al. (1999) used Eigen System Realization Algorithm and observer/Kalman filter identification approach to evaluate the same bridge system. Tsai et al. (1993) studied Caltrans seismic evaluation procedures on bridge structures using five different short bridge over-crossings concluding consistency with observed performances.

Several studies for analyzing recorded bridge data around the world are published in the literature. Chaudhary et al. (2000) used ground motion recordings from Kobe earthquake to determine vibration properties of two base-isolated bridges. Loh and Lee (1997) assessed the properties of New Lian River Bridge in Taiwan using weak and strong ground excitations by conducting multi-input/single-output identification.

The present paper covers the application of System Identification (SI) techniques on representative seven bridges out of the 54 instrumented ones in California. The primary aim of the study is to determine fundamental frequencies of these bridges to form the knowledge through which design recommendations are assessed. In addition, it is possible through SI methods to determine modal shapes and damping ratios. In this paper representative examples of such analysis concentrating on the evaluation of the first few modes of a complex curved bridge system is also presented. Note that, throughout the paper, extensive use of reports by Safak (1991), Fenves and Desroches (1994) and Glaser (1998) is made. These reports provide valuable information for performing parametric analysis using discrete time filters for structural systems.

After this introduction, the paper presents a concise information on the selected bridges. This is followed by a brief insight into the used system identification methods. Subsequently, the results of the data analysis, with detailed presentation on selected two bridges, namely, Truckee I80/Truckee River Bridge and Sylmar I5/14 Interchange Bridge are presented. Afterwards, the results from analytical modeling of the considered bridge systems using finite element method including comparison with the identified properties from the data analysis are given. Finally, the paper ends with concluding remarks and proposed future work.

SELECTED BRIDGES

The selected bridges and relevant information including earthquake data are listed in Tables 1 and 2. The criterion for choosing these bridges was to have a representative sample of commonly used systems in California. The selected bridges had different characteristics including: material (reinforced concrete versus prestressed concrete), bent types (single-column versus multiple-columns), number of spans (2 to 9), section types (box girders with different cell numbers), soil properties (soft versus stiff), structural

systems (continuous versus simply supported), and orientation (straight, skewed, and curved). Moreover, availability of sufficient sensors governed the choice of the bridges.

Table 1: Selected Bridge Information

Bridge	*Structural System*	*Built*	*Instr.*	*Spans*	*Chan.*
Hayward BART elevated section	Simply supported P/C twin beams on R/C single columns with double cantilevers	1967	1986	3 instrum. @ 77' each	19
Lake Crowley-Hwy 395	Continuos R/C 5-cell box girder on abutments and a 2-column bent	1969	1995	2 @ 104' & 99'	9
El Centro Hwy 8/Meloland Overpass	Monolithic continuous R/C 3-cell box girder on abutments and a single column bent	1971	1978	2 @ 104'	32
Rio Dell–Hwy 101/Painter St. Overpass	Continuous R/C 6-cell box girder on abutments and a 2-column bent	1976	1977	2 @ 119' & 146'	20
Ridge Crest-Hwy 580/13 Interchange	Continuos R/C 5-cell box girder on abutments and a 2-column bent	1966	1996	4 @ 62', 83', 83' & 54'	9
Truckee-I80/Truckee River Bridge	Continuos R/C 3-cell box girder on inverted A-column bents	1989	1995	3 @ 185', 192' & 185'	8
Sylmar I5/14 Interchange	Continuous R/C 3-cell box girder on single column bents with an expansion joint	1994	1995	9 from 135' to 198'	38

Table 2 Earthquake data investigated

Bridge	*Earthquake Date*	*Max. Free Field Acc.(g)*	*Max. Structure Hrz. Acc. (g)*
Hayward BART	10/17/1989	0.160	0.508
Lake Crowley-Hwy 395	06/08/1998	0.200	0.244
	06/14/1998	0.231	0.405
	05/15/1999	0.092	0.270
El Centro Hwy 8/Meloland Overpass	04/09/2000	0.043	0.174
	06/14/2000	0.013	0.044
	06/14/2000	0.011	0.038
Rio Dell–Hwy 101/Painter St. Overpass	07/31/1987	0.141	0.335
	11/21/1986	0.432	0.399
	04/25/1992	0.543	1.089
Ridge Crest-Hwy 580/13 Interchange	05/06/1997	0.005	0.016
	03/05/1998	0.019	0.077
Truckee-I80/Truckee River	10/30/1998	0.088	0.172
Sylmar I5/14 Interchange	04/11/1999	0.011	0.066
	10/16/1999	0.019	0.052

METHODOLOGY

The total displacement of the structure is represented as follows,

$$\ddot{u}_T = \ddot{u} + r\,\ddot{u}_g \tag{1}$$

where, $\ddot{u}_T$, $\ddot{u}$, and $\ddot{u}_g$ are the total structural acceleration, the relative structural acceleration, and the ground acceleration, respectively and r is the influence matrix. Using modal equations (Chopra, 1995) and classical damping, $\ddot{u}$ can be expressed by superposition of different modes as follows.

$$\ddot{u}(t) = \sum_{j=1}^{J} \phi_j \, \ddot{X}_j(t) \tag{2}$$

where ϕ_j is the j^{th} mode shape with modal coordinate $\ddot{X}_j(t)$ which can be obtained from the solution of the following differential equation.

$$\ddot{X}_j(t) + 2\xi_j \omega_j \dot{X}_j(t) + \omega_j{}^2 X(t) = -\frac{1}{M_j} L_j{}^T \ddot{u}_g{}^T \tag{3}$$

where ξ_j, ω_j, M_j are the j^{th} modal damping, frequency, and mass, respectively and L_j is the j^{th} vector of generalized influence factors for support motion. In the frequency domain, the solution of equation (3) is written using Laplace transform as follows.

$$\overline{X}(s) = -\frac{1}{s^2 + 2\xi_j \omega_j s + \omega_j{}^2} \frac{1}{M_j} L_j{}^T \, \overline{\ddot{u}}_g(s) \tag{4}$$

From the above equations, one obtains,

$$\overline{\ddot{u}}_T(s) = H(s) \; \overline{\ddot{u}}_g(s) \tag{5}$$

where,

$$H(s) = \sum_{j=1}^{J} \left(\frac{2\xi_j \omega_j s + \omega_j{}^2}{s^2 + 2\xi_j \omega_j s + \omega_j{}^2} \right) \frac{\phi_j{}^T L_j}{M_j} \tag{6}$$

<u>Non-Parametric Evaluation</u>

Transfer functions are used as for estimating system modal frequencies. For stationary input signals the transfer function may be defined in one of the following two ways.

$$H_1(i\omega) = S_{yx}(\omega) / S_{xx}(\omega) \tag{7}$$

$$H_2(i\omega) = S_{yy}(\omega) / S_{xy}(\omega) \tag{8}$$

where, S_{xx} and S_{yy} are the auto-power spectra, Fourier transform of the autocorrelations of input signal x and output signal y, respectively. S_{yx} and S_{xy} are the cross-power spectra, Fourier transform of the cross-correlations between x and y. It is known that H_1 estimate is more prone to input noise, whereas H_2 estimate is more prone to output noise. The square root of the ratio between H_1 and H_2, (Equation (9)), i.e. coherency (γ), gives an important quantity for evaluating the noise in the measurements.

$$\gamma = \sqrt{H_1(i\omega) / H_2(i\omega)} \tag{9}$$

In general, CSMIP data has bandwidth of 0.1 to 50 Hz. Since 50 Hz is much larger than the subject frequencies, the data is first low pass filtered (Ljung, 1997). In addition, the data is decimated to one-fourth the size after the filtering. Note that for older data, where the frequency resolution is not adequate, decimation is performed to one-half the size. The data is processed also by Welch method (Ljung, 1997) for estimating spectral densities using 3 to 5 data windows. Frequency resolution and windowing selection is chosen different for each earthquake record considering the quality of the data and the required resolution.

Parametric Identification

Transfer function provides accurate identification of the frequency and the mode shape information for the first few modes. A more accurate alternative would be the use of linear discrete time models, which yield both frequency and damping information. Typical single-input/single-output discrete time filter is defined as follows.

$$y_t = b_0 x_t + b_1 x_{t-1} + \cdots + a_1 y_{t-1} + a_2 y_{t-2} \tag{10}$$

where y_t and x_t are the output and input of the system at time t, respectively. The input series "b" coefficients are the causal Moving Average (MA) process, and the output series "a" coefficients are the non-causal Auto-Regressive (AR) process. Taking the Fourier transform of the above expression and applying the Z-transform gives the transfer function for this discrete system.

$$H(\omega) = \frac{Y_\omega}{X_\omega} = \frac{b_0 + b_1 z + b_2 z^2 + \cdots}{1 + a_1 z + a_2 z^2 + \cdots} \tag{11}$$

Various forms of the method exist in terms of modeling the error of the system. General format of a multi-input/single-output system can be given in a polynomial form as in Equation (12).

$$A(z)\, y(t) = \sum_{i=1}^{NI} [B_i(z)/F_i(z)]\, x_i(t - \delta_i) + [C(z)/D(z)]\, e(t) \tag{12}$$

where A, B, C, D, and F are polynomials in terms of the shift operator (z) to define various system properties and $e(t)$ is the prediction error in the model. δ is the time delay in the input. The summation in Equation (12) is performed for the number of inputs (NI).

The output error and the Auto-Regressive eXtended (ARX) model are selected in this study as best fits are acquired with these methods. In Equation (12), the output error models correspond to the case of A, C, and D being ones, while the ARX models correspond to the C, D, and F being ones. The parameters of the polynomials A, B, and F are estimated using least square minimization of the prediction error (e) (Ljung, 1997).

The modal frequencies of the dynamic system can be acquired from the poles of the transfer function between the different inputs and the output. The poles are the roots of the denominators, which exist in n/2 complex conjugate pairs where n is the order of

the auto-regressive part of each model. These can be transformed to the poles of the transfer function defined in Equation (6) using the transformation,

$$s_j = \ln(z_j)/\Delta t \tag{13}$$

where Δt is the sampling interval. Subsequently, one obtains the following relation

$$s_j, s_j^* = -\xi_j \omega_j \pm i\omega_j \sqrt{(1-\xi_j^2)} \tag{14}$$

Finally, the modal frequencies and damping ratios for the considered n/2 modes can be determined as follows.

$$\omega_j = \sqrt{(s_j \; s_j^*)} \tag{15}$$

$$\xi_j = -\mathrm{Re}(s_j)/\omega_j \tag{16}$$

The simulated and recorded outputs are compared to assess the quality of the model. This is conducted using the normalized mean square error, *J*, defined in (Werner et al., 1985).

$$J = \sum_{i=1}^{N} (y_i - y_i^M)^2 \Big/ \sum_{i=1}^{N} (y_i)^2 \tag{17}$$

where y_i *and* y_i^M are original recording from the structure and model output, respectively and *N* is the total number of time steps. A value of *J* less than 0.1 is defined to be excellent, whereas *J* in the range of 0.1 to 0.5 is considered adequate. Time history fits with *J* more than 0.5 are poor and disregarded in the analysis.

Most of the selected bridges are analyzed using multi-input/single-output error model. In part of the selected bridges, the sensor numbers and locations did not permit such analysis. The orientation of the sensors used in the SI is according to Figure 1 where the input sensors are denoted A, B, and C whereas the output sensor is denoted D.

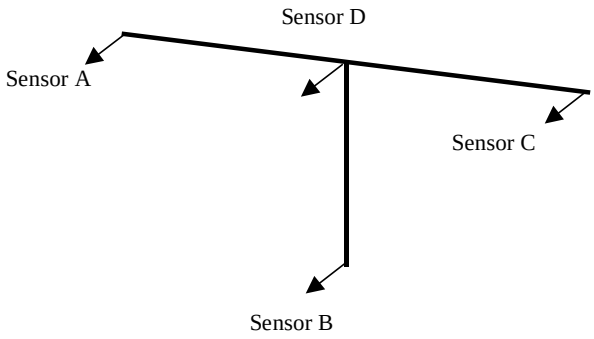

Figure 1 Selected pattern of sensors for identification

For the output error models, the acquired frequencies and damping ratios are for each of the input/output pairs. As three inputs and single output are used in this study, the frequency and damping values between the ground input and the superstructure output are selected to be the best candidate for estimating the system vibration characteristics. For the ARX models, single group of frequencies and damping ratios are acquired from the whole structure using the same sensor arrangement.

SYSTEM IDENTIFICATION

Hayward BART Elevated Section

The structural configuration of Hayward BART elevated section is illustrated in Figure 2. The SI results are given in Tables 3 and 4 for the longitudinal and transverse directions, respectively. Although the fundamental frequency in the longitudinal direction is 1.00 Hz, the third mode corresponding to 3.50 Hz is the dominant mode because of the high coupling provided by BART station nearby and the railing on structure. For the transverse direction, the fundamental frequency is found to be 1.67 Hz.

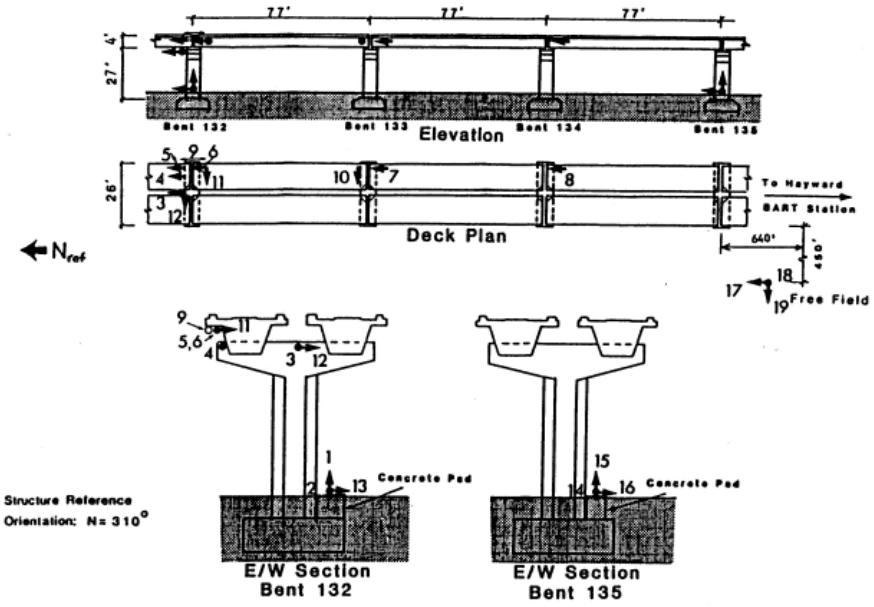

Figure 2 Hayward BART Elevated Section

Table 3 SI of Hayward BART Elevated Section (Longitudinal)

EQ. Date	*Mode #*	*TFE*	*OUTPUT ERROR*	
		Frequency	*Frequency*	*Damping*
10/17/1989	1	1.00	-	-
	2	2.10	2.07	2.12
	3	3.50	3.61	1.08

Table 4 SI of Hayward BART Elevated Section (Transverse)

Eq. Date	*Mode #*	*TFE*	*OUTPUT ERROR*	
		Frequency	*Frequency*	*Damping*
10/17/1989	1	1.80	1.67	6.20
	2	3.60	3.60	39.49

Lake Crowley–Highway 395 Bridge

The structural configuration of Lake Crowley-Highway 395 Bridge is illustrated in Figure 2. The SI results are given in Table 5. The fundamental frequency of the structure is found to be 4.6 Hz. For the second earthquake, as shown in Table 5, the first frequency was not identified since the ground motion has a very high peak of 4.9 Hz in the frequency domain, exciting the structure primarily in the corresponding mode.

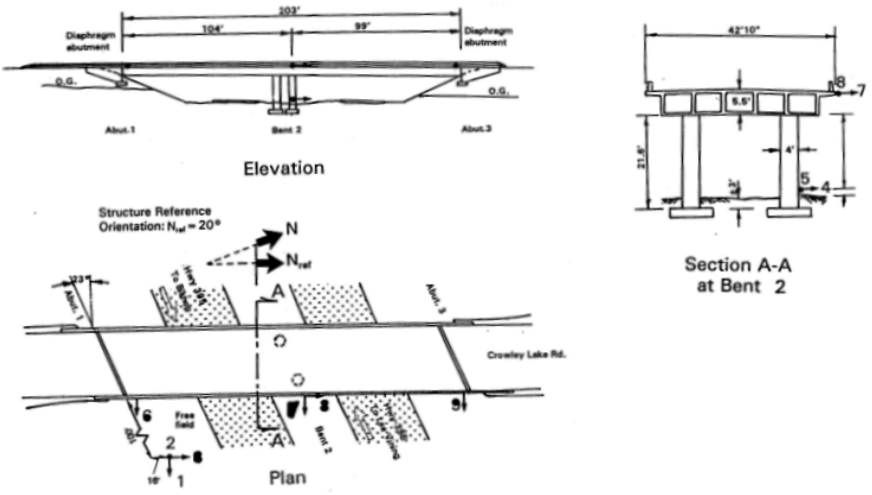

Figure 3 Lake Crowley-Highway 395 Bridge

Table 5 SI of Lake Crowley-Hwy 395 Bridge

EQ. Date	*Mode #*	*TFE*	*OUTPUT ERROR*		*ARX*	
		Frequency	*Frequency*	*Damping*	*Frequency*	*Damping*
06/08/1998	1	4.60	4.49	5.62	-	-
	2	4.99	-	-	-	-
	3	5.90	5.91	1.21	-	-
06/14/1998	1	-	-	-	-	-
	2	4.90	4.98	0.56	4.80	8.74
	3	6.06	6.37	4.04	6.15	4.38
05/15/1999	1	4.70	4.49	6.24	4.74	8.92
	2	4.98	4.94	1.21	-	-
	3	6.50	6.29	6.81	5.64	3.86

El Centro–Highway 8/Meloland Overpass

The structural configuration of El Centro–Highway 8/Meloland Overpass is illustrated in Figure 2. The SI results are given in Table 6. The fundamental frequency of the structure was deemed to be 3.25. As the bridge is monolithic with the abutments, the mode shapes involve embankment movements. Werner et al. (1987) determined modal frequencies of 2.50 and 3.20 for the case involving embankment movements, and 3.70 for

the case involving only superstructure. Note that there is significant difference between the amplitude of the bridge motion in the current study compared to that by Werner et al. (1987).

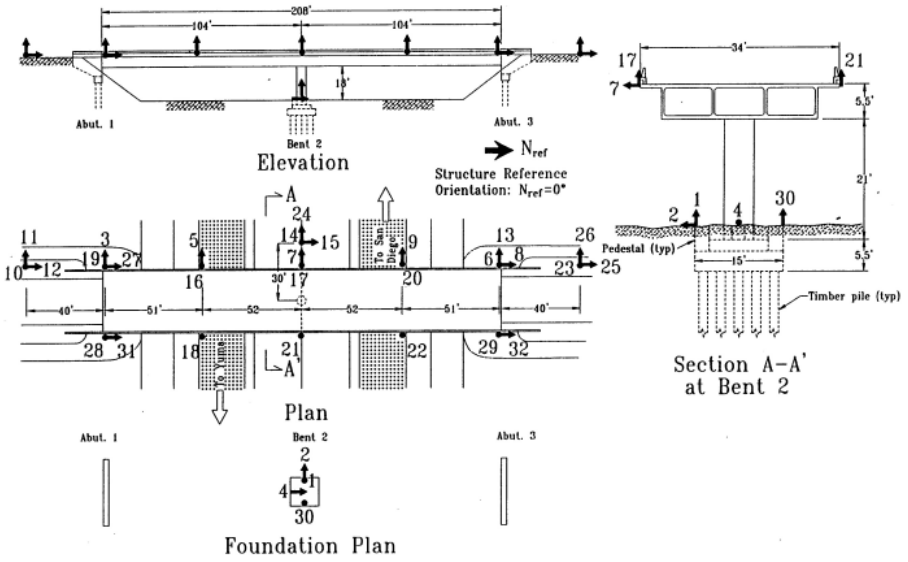

Figure 4 El Centro-Highway 8/Meloland Overpass

Table 6 SI of Meloland Overpass

EQ. Date	*Mode #*	*TFE*	*OUTPUT ERROR*		*ARX*	
		Frequency	*Frequency*	*Damping*	*Frequency*	*Damping*
04/09/2000	1	3.15	3.08	4.36	3.24	7.72
	2	3.77	-	-	3.73	5.20
06/14/2000	1	3.18	3.33	24.27	3.27	35.81
	2	3.91	3.86	5.18	3.82	3.59
06/14/2000	1	3.28	3.30	3.12	3.23	14.67
	2	3.90	3.96	5.21	3.99	2.83

Rio Dell–Highway 101/Painter Street Overpass

The structural configuration of Rio Dell–Highway 101/Painter Street Overpass is illustrated in Figure 5. The SI results are given in Table 7. The fundamental frequency of the system is determined to be 3.5 Hz. For the third earthquake, the SI results are significantly different from the first two earthquakes. This is expected since the maximum acceleration of the superstructure reaches 1.09 g during the third earthquake indicating high chance of change in the system properties.

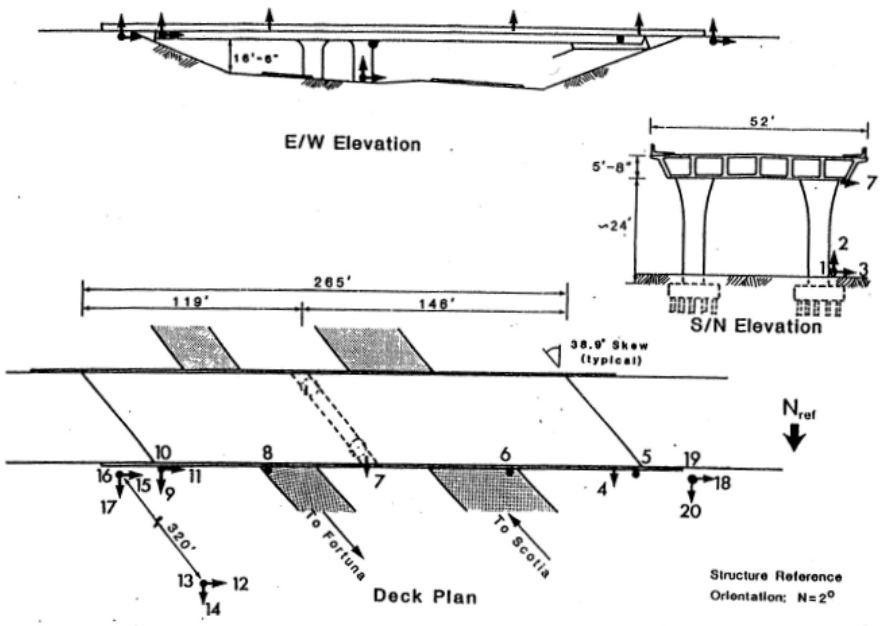

Figure 5 Rio Dell-Highway 101/Painter Street Overpass

Table 7 SI of Rio Dell-Hwy 101/Painter Street Overpass

EQ. Date	*Mode #*	*TFE*	*OUTPUT ERROR*		*ARX*	
		Frequency	*Frequency*	*Damping*	*Frequency*	*Damping*
07/31/1987	1	3.56	3.33	0.66	3.45	10.04
	2	4.74	4.86	2.1	4.82	4.11
11/21/1986	1	3.51	3.50	13.79	3.27	35.81
	2	-	-	-	4.74	6.18
04/25.1992	1	2.95	-	-	3.09	33.12
	2	4.15	-	-	4.15	7.31

Ridgecrest–Highway 395/Brown Road Bridge

The structural configuration of Ridgecrest–Highway 395/Brown Road Bridge is illustrated in Figure 6. The SI results are given in Table 8. The fundamental frequency is determined to be 3.22 Hz for this bridge. The results from the output error model using the second earthquake for this bridge is decided as more representative results. On the other hand, the ARX model inaccuracy for the second earthquake is evidenced by the relatively high error of this model for this particular case.

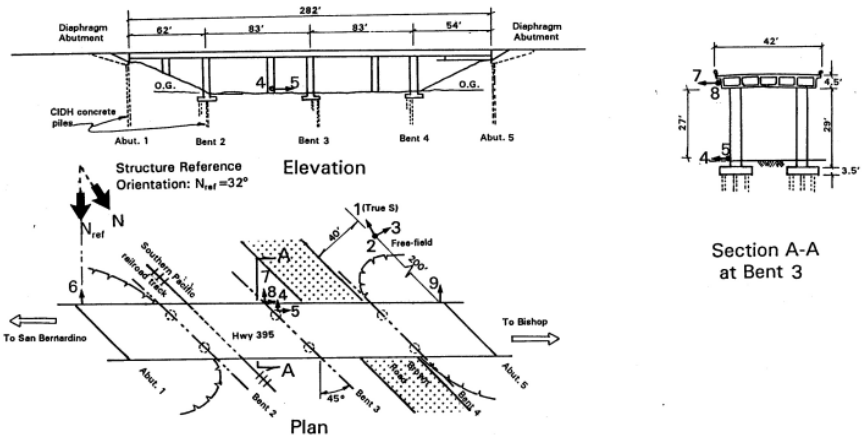

Figure 6 Ridgecrest-Highway 395/Brown Road Bridge

Table 8 SI of Ridgecrest-Hwy 395/Brown Road Bridge

EQ. Date	*Mode #*	*TFE*	*OUTPUT ERROR*		*ARX*	
		Frequency	*Frequency*	*Damping*	*Frequency*	*Damping*
05/06/1997	1	3.57	3.36	1.88	3.68	1.76
03/05/1998	1	3.21	3.22	1.80	3.39	5.34

Truckee-I80/Truckee River Bridge

The structural configuration of Truckee-I80/Truckee River Bridge is illustrated in Figure 7. The SI results are given in Table 9. The fundamental mode for the bridge is determined to be 1.19 Hz. The output error model did not identify some of the higher modes whereas ARX model was successful in that respect.

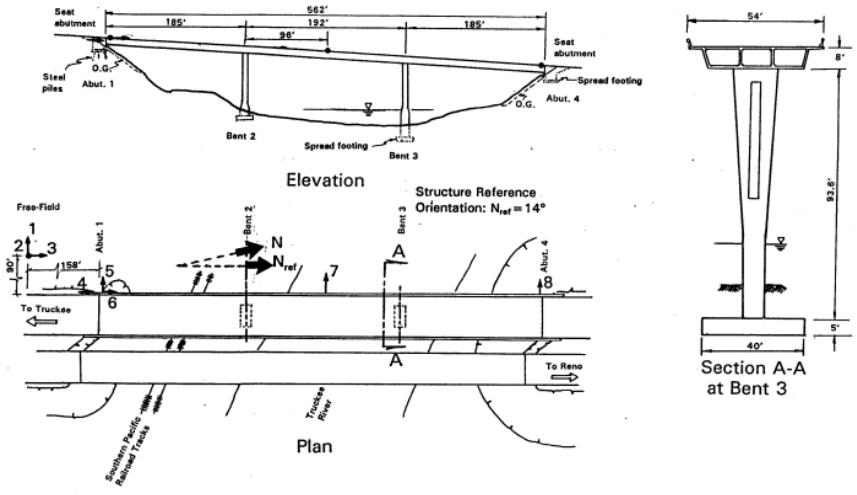

Figure 7 Truckee-I80/Truckee River Bridge

Table 9 SI of Truckee-I80/Truckee River Bridge

EQ. Date	*Mode #*	*TFE*	*OUTPUT ERROR*		*ARX*	
		Frequency	*Frequency*	*Damping*	*Frequency*	*Damping*
10/30/1998	1	1.12	1.19	2.30	1.19	2.82
	2	2.27	-	-	2.12	10.33
	3	3.13	-	-	3.02	2.48
	4	4.15	4.18	1.31	4.22	2.68
	5	6.54	6.36	0.45	-	-

Figure 8 represents a comparison for transverse acceleration at the middle of the deck (Channel 7 as shown in Figure 7) between the recorded and simulated (using ARX model) time histories. This figure illustrates excellent fit as also evidenced from the normalized mean square error (J = 0.022).

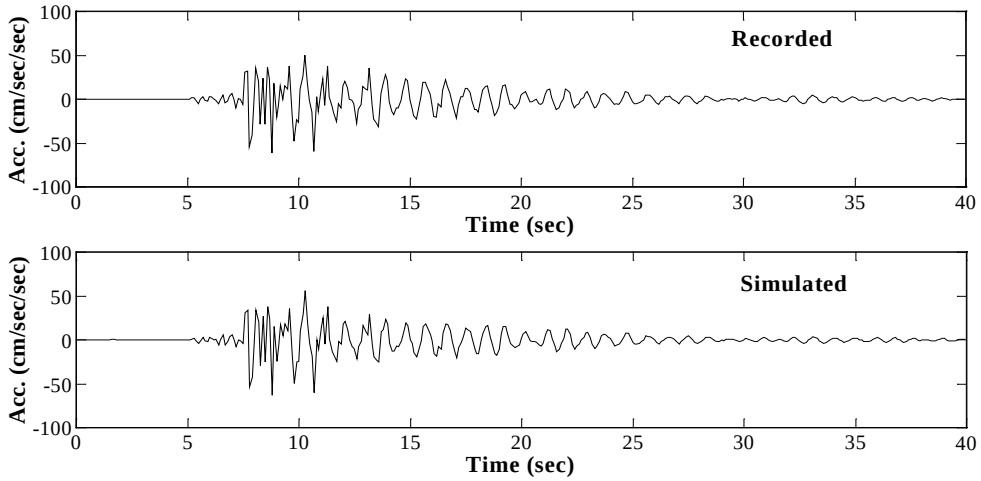

Figure 8 Time History Comparison, ARX Model versus Recording

Sylmar-I5/14 Interchange Bridge

The structural configuration of Sylmar-I5/14 Interchange Bridge is illustrated in Figure 9. The large size and geometrical configuration (e.g. the expansion joint in the middle of the bridge) of the bridge system led to the analysis of the bridge in two parts, namely the North and South substructures (left and right of the expansion joint). The SI results are given in Tables 10 and 11 for the South and North substructures, respectively.

The fundamental frequency in the first earthquake for the bridge system is identified to be 0.78 Hz from the North substructure. On the other hand, it is identified that the lowest frequency from the South substructure is 0.97 Hz corresponding to the second (anti-symmetric) mode of the whole bridge system. From Tables 10 and 11, it is noticed that the higher frequencies (> 1 Hz) are equally identified from both the North and South substructures.

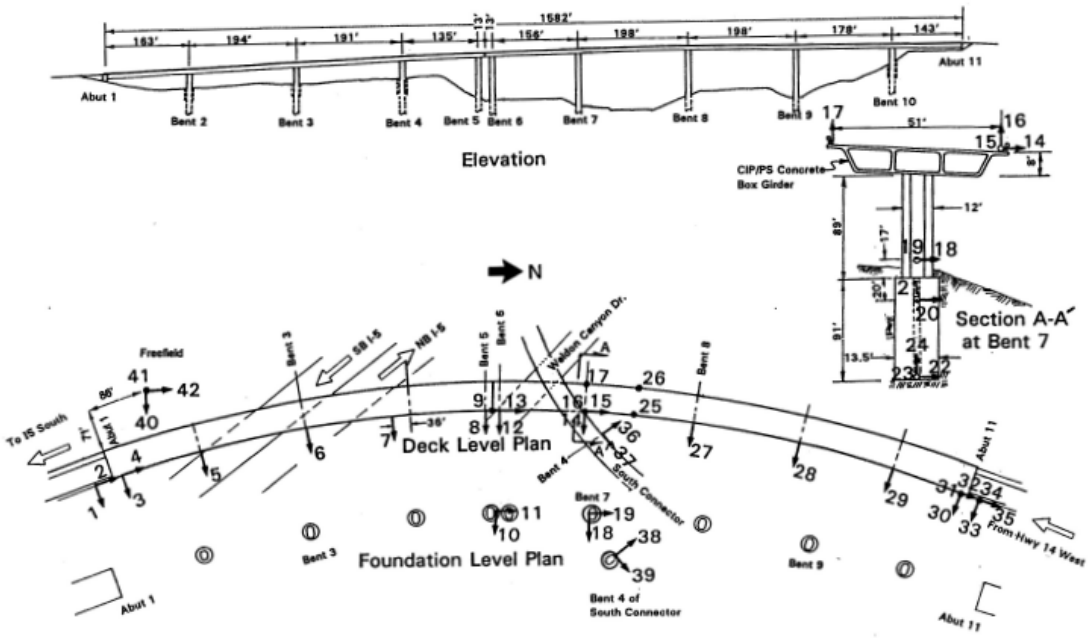

Figure 9 Sylmar-I5/14 Interchange Bridge

The fundamental frequency and the higher ones are lower based on SI using data from the second earthquake. This observation is attributed to the shear key at the expansion joint binding in the second earthquake, which is not the case during the first one. The maximum displacements near the expansion joint in the first and the second earthquakes are 0.05 cm and 2.91 cm, respectively. From the visual inspection of the displacement time histories, significant differences are observed in the structural response near the expansion joint for the two earthquakes (refer to Figure 10).

Table 10 SI of Sylmar-I5/14 Interchange Bridge (South Substructure)

EQ. Date	*Mode #*	*TFE*	*OUTPUT ERROR*		*ARX*	
		Frequency	*Frequency*	*Damping*	*Frequency*	*Damping*
04/11/1999	1	0.97	1.01	3.03	-	-
	2	1.25	1.33	3.22	-	-
	3	1.61	-	-	-	-
	4	1.76	-	-	-	-
	5	2.22	2.21	3.79	-	-
	6	2.73	-	-	-	-
10/16/1999	1	0.90	0.84	57.16	0.88	22.76
	2	1.06	1.04	13.50	-	-
	3	1.32	-	-	1.4450	8.94
	4	1.54	1.64	7.26	-	-
	5	-	2.05	7.88	2.0209	2.35
	6	2.63	2.39	1.13	2.6537	2.53

Table 11 SI of Sylmar-I5/14 Interchange Bridge (North Substructure)

EQ. Date	*Mode #*	*TFE*	*OUTPUT ERROR*		*ARX*	
		Frequency	*Frequency*	*Damping*	*Frequency*	*Damping*
04/11/1999	1	0.78	0.77	0.94	0.74	9.06
	2	0.97	-	-	-	-
	3	1.27	1.20	3.95	1.20	14.43
	4	-	-	-	1.86	2.08
	5	2.27	2.07	1.37	-	-
	6	-	2.60	0.32	2.52	18.19
10/16/1999	1	0.71	0.70	3.76	0.69	81.65
	2	0.90	-	-	-	-
	3	1.04	-	-	-	-
	4	-	1.30	5.96	1.32	21.15
	5	1.56	-	-	1.84	7.16
	6	-	2.07	9.16	2.15	7.42

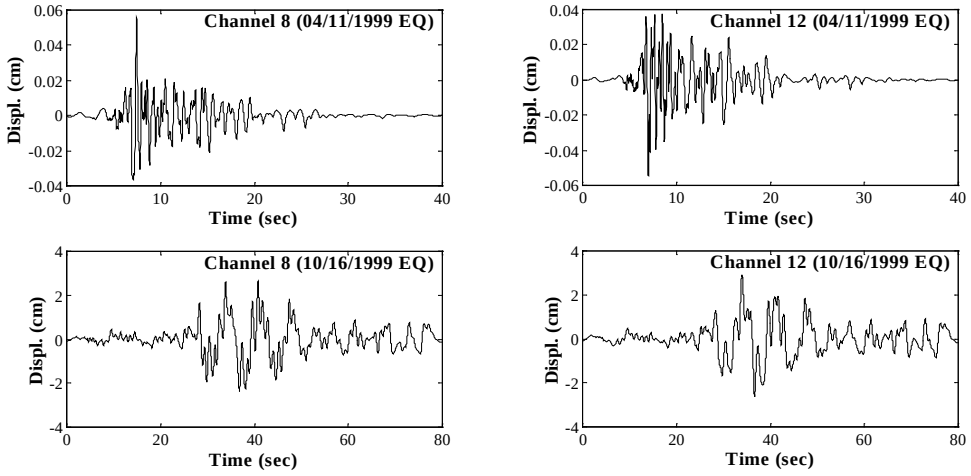

Figure 10 Displacement Time Histories at Sylmar Expansion Joint

The transverse acceleration time histories from the North substructure (channel 14 from Figure 9) from the first earthquake are compared in Figure 11 for the recorded data and simulated output using ARX model. From this figure, it is evidenced that the fitting is excellent (J = 0.025).

Assessment of Error in the SI Models

The errors for the SI models are within acceptable limits. Apart from the single analysis on Ridgecrest, all the multi-input/single-output error values are about or under 0.04. For BART, only single-input/single-output analysis is performed. The error, although significantly more than the multi-input approach, is better compared with the

results of the single-input/single-output analysis performed on the other bridges in this study. The errors of the multi-input/single-output analysis with respect to each of the selected bridges and with respect to the maximum acceleration recorded at the output sensors are given in Figures 12 and 13.

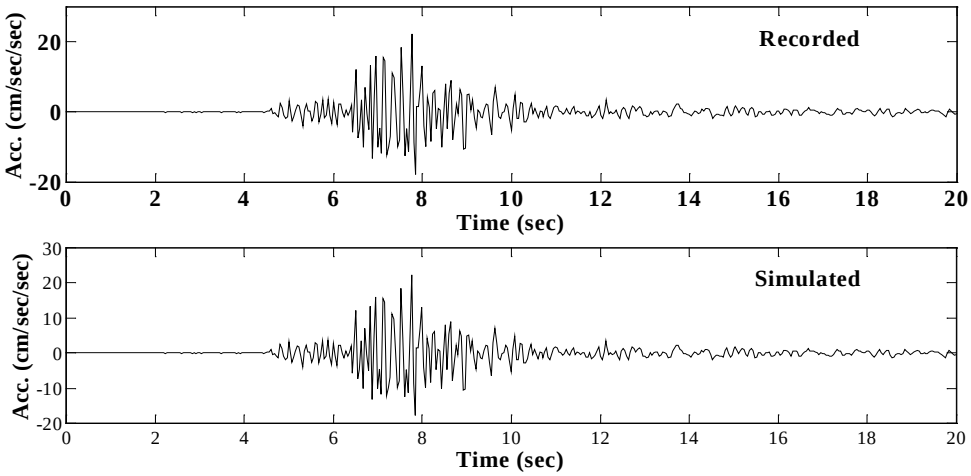

Figure 11 Time History Comparison, ARX Model versus Recording

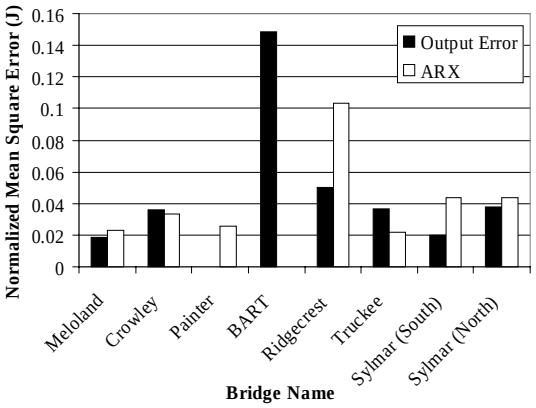

Figure 12 NMSE for SI of Bridges

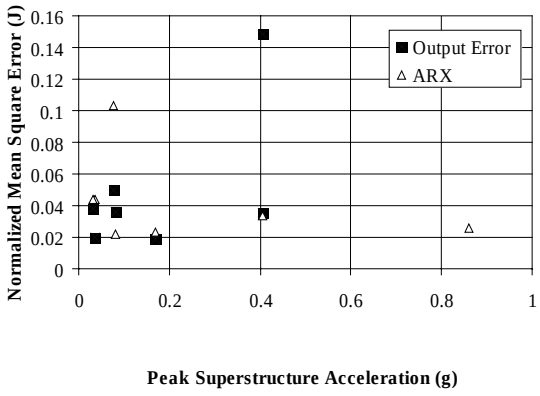

Figure 13 NMSE versus Peak Acceleration

FINITE ELEMENT ANALYSIS

Six of the selected seven bridges were analyzed using Finite Element Analysis (FEA) where Eigen analyses were conducted. The analyses are performed using the finite element package DIANA (Witte and Feenstra, 1998). The results of these FEA compared with those from the SI are given in Table 12. The analysis of Hayward BART elevated segment required high mass and stiffness coupling to match the SI results. In this way,

the fundamental frequencies in the longitudinal and transverse directions were determined. In the case of Lake Crowley-Highway 395 Bridge, Caltrans design abutment stiffness provisions (Caltrans, 1999, Priestley et al., 1996) did not lead to reasonable results compared to the SI. When the boundary conditions of the system was treated as fixed, the fundamental frequency was accurately determined. Caltrans abutment stiffness gave a perfect match with the acquired frequency from the SI for El Centro Hwy 8/Meloland Overpass. Rio Dell- Highway 101/Painter Street Overpass had the same problem as Lake Crowley-Highway 395 Bridge. Caltrans abutment stiffness estimation for the analysis of Rio Dell- Highway 101/Painter Street Overpass led to significantly lower frequencies whereas assuming the boundary condition for the abutment fixed led to the value of the fundamental frequency from SI.

Table 12 Comparison between FEA and SI

Bridge	f_1 *(Hz) SI*	f_1 *(Hz) FEM*	*Remarks*
Hayward BART	1.67	1.95	High mass and stiffness coupling
Lake Crowley-Hwy 395 Overpass	4.50	4.46	Fixed Boundaries
El Centro Hwy 8/Meloland Bridge	3.20	3.25	Excellent agreement using abutment stiffness based on Caltrans
Rio Dell–Hwy 101/Painter Street Overpass	3.50	3.55	f_1 =2.53 using Caltrans abutment stiffness, improved results with fixed east boundary
Truckee-I80/Truckee River Bridge	1.09	1.15	Caltrans abutment stiffness with cracked column section (I_{eff}/I_{gross}=0.35)
Sylmar I5/14 Interchange	0.71	0.72	Intermediate hinge at expansion joint with cracked column section (I_{eff}/I_{gross}=0.45)

The FEA of the two taller bridges, namely Truckee-I80/Truckee River Bridge and Sylmar I5/14 Interchange, required the use of cracked column cross sections for better match with the SI results. Caltrans design aids for the effective moment of inertia of cracked column sections (based on the axial load and the longitudinal reinforcement ratios) (Caltrans, 1999) were followed. Moreover, Caltrans abutment stiffness provisions were adequate for modeling Truckee-I80/Truckee River Bridge (refer to Figure 14).

Sylmar-I5/14 Interchange is modeled with the expansion joint in between the North and South substructures as an intermediate hinge (refer to Figure 15). It can be deduced that the first mode of the system is a local mode of the flexible North substructure, which is weak in the South substructure. This behavior, first determined from the SI of the system, is also captured using FEA. The second mode which appears to

be the dominant mode in the South substructure is actually the second (anti-symmetric) mode for the whole bridge system with a node existing in the North span.

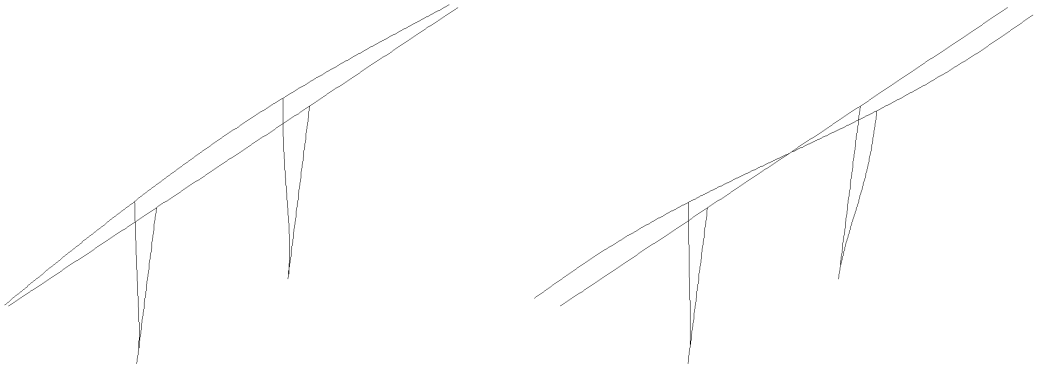

First Mode (f_1 = 1.15 FEA, 1.09 SI) Second Mode (f_2 = 1.95 FEA, 2.15 SI)

Figure 14 Modal Shapes of Truckee-I80/Truckee River Bridge

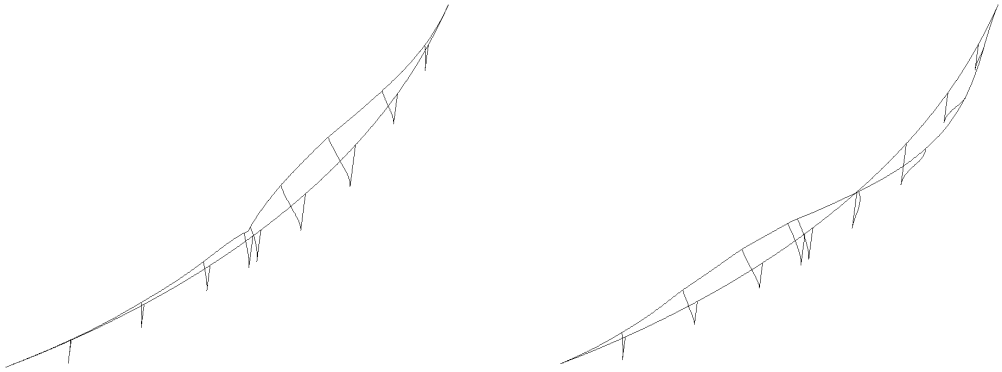

First Mode (f_1 = 0.72 FEA, 0.71 SI) Second Mode (f_2 = 1.00 FEA, 0.90 SI)

Figure 15 Modal Shapes of Sylmar I5/14 Interchange

CONCLUDING REMARKS

From the above results and discussions, the following conclusions may be inferred:

1. The selected seven bridges form a representative sample of common bridge systems in California. They accounted for different materials, section shapes, soil conditions, and structural configurations. Moreover, the data from several earthquakes was examined.
2. The utilized system identification methods are shown to be powerful techniques in identifying frequencies, mode shapes, and damping ratios for the available number and orientation of sensors.
3. The model errors (using the normalized mean square error) for both output error and ARX methods are within acceptable limits. It is worth mentioning that the ARX method is more robust and capable of accurately identifying more modes than the

output error method. In general, ARX identified higher damping ratios than the output error method.

4. The fundamental frequencies based on Eigen analysis using the finite element method reproduced the system identification results with reasonable accuracy. This was achieved with proper boundary conditions and column cross section properties.
5. Caltrans design aids for the effective moment of inertia when used for tall column cross sections led to reasonable analytical predictions of the fundamental frequency. On the contrary, the Caltrans provisions for the abutment stiffness require further refinement particularly for short span bridges, e.g. Lake Crowley-Hwy 395 Bridge.

ACKNOWLEDGMENTS

The authors gratefully acknowledge the financial support provided by the California Strong Motion Instrumentation Program under the Contract No. 1098-714 with funding from the California Department of Conservation. The contents of this paper do not necessarily represent the policy of the funding agency. The technical support of Dr. Moh Huang and Mr. Patrick Hipley was instrumental for the completion of the research.

REFERENCES

1. Abdel-Ghaffar, A.M., Niazy, A.M., and Masi, S.F. (1993) “Analysis of the seismic records of a suspension bridge,” Proceedings of the ASCE structural congress ’93, New York, 2, 1509-1514.
2. Caltrans (1999) “Caltrans Seismic Design Criterion,” Version 1.1, July.
3. Chaudhary, M.T.A., Abe, M., Fujino, Y., and Yoshida, J. (2000) “System identification of two base-isolated bridges,” Accepted for Journal of Engineering Mechanics, ASCE.
4. Chopra, A. K. (1995) “Dynamics of Structures,” Prentice Hall, New Jersey.
5. Goel, R.K. and Chopra, A.K. (1995), “Seismic response study of the Hwy 101/ Painter Street Overpass near Eureka using strong-motion records,” Data Utilization Report CSMIP/ 95-01.
6. Fenves, G.L. and Desroches, R. (1994) “Response of the northwest connector in the Landers and Big Bear earthquakes,” Report No. 94/12, Earthquake Engineering Research Center, University of California, Berkeley, CA.
7. Fenves, G.L., Filippou, F.C., and Sze, D. (1992) “Response of the Dumbarton Bridge in the Loma Prieta earthquake,” Report No. 92/02, Earthquake Engineering Research Center, University of California, Berkeley, CA.
8. Glaser, S.D. (1998) “ System identification and its application to soil dynamics,” Report No. 98/01, Geotechnical Engineering, University of California, Berkeley, CA.
9. Hipley, P, Huang., M., and Shakal, A. (1998) “ Bridge instrumentation and post-earthquake evaluation of bridges”, Proceedings SMIP98 seminar on utilization of strong motion data, 53-71.

10. Levine, M.B. and Scott, R.F. (1989) “Dynamic response verification of simplified bridge-foundation model,” Journal of Geotechnical Engineering, 115, 2, 246-260.
11. Ljung, L. (1997) “System Identification Toolbox Users Guide,” The Math Works Inc.
12. Loh, C.H. and Lee, Z.K. (1997) “Seismic monitoring of a bridge: Assessing dynamic characteristics from both weak and strong ground motions,” Earthquake Engineering and Structural Dynamics, 26, 269-288.
13. Lus, H., Betti, R., and Longman, R.W. (1999) “Identification of linear structural systems using earthquake induced vibration data,” Earthquake Engineering and Structural Dynamics, 28, 1449-1467.
14. McCallen, D.B. and Romstadt, K.M. (1994) “Dynamic analysis of a skewed short span box girder overpass,” Earthquake Spectra, 10(4), 729-755.
15. Priestley, M.J.N., Seible, F., and Calvi, G.M. (1996) “Seismic Design and Retrofit of Bridges,” John Wiley & Sons, Inc., New York.
16. Saadeghvaziri, M.A., and Foutch, D.A., (1989) ” Effects of vertical motion on the inelastic behavior of highway bridges,” Structures Congress '89: Seismic engineering: research and practice, ASCE, New York, 51-61.
17. Safak, E. (1991) “Identification of linear structures using discrete-time filters,” Journal of Structural Engineering, ASCE, 117(10), 3064-3085.
18. Safak, E. (1994) “Use of structural response data from small earthquakes and aftershocks,” NIST SP 871, Wind and Seismic Effects, Proceedings of the 26th Joint Meeting of the U.S.-Japan Cooperative Program in Natural Resources Panel on Wind and Seismic Effects, NIST, Gaithersburg, Maryland, 613-623.
19. Tsai, N.C., Firouz, A., Sedarat. H., Nisar, A., and Werner, S.D. (1993) “ Application of Caltrans current seismic evaluation procedures to selected short bridge overcrossing structures,” Technical Report, Dames & Moore.
20. Tseng, W.S., Yang, M.S., Penzien, J. (1992) “Seismic performance investigation of the Hayward BART elevated section,” Data Utilization Report CSMIP/ 92-02.
21. Werner, S.D., Beck, J.L., and Levine, M.B. (1987) “Seismic response evaluation of Meloland Road Overpass using 1979 Imperial Valley earthquake records,” Earthquake Engineering and Structural Dynamics, 15, 249-274.
22. Werner, S.D., Crouse, C.B., Katafygiotis, L.S., and Beck, J.L. (1994) “Use of strong motion records for model evaluation and seismic analysis of a bridge structure,” Proceedings of the Fifth U.S. National Conference on Earthquake Engineering, 1, 511-520.
23. Wilson, J.C. (1986) “Analysis of the observed seismic response of an highway bridge,” Earthquake Engineering and Structural Dynamics, 14, 339-354.
24. Wilson, J. C. and Tan, B.S. (1990) “Bridge abutments: assessing their influence on earthquake response of Meloland Road Overpass,” Journal of Engineering Mechanics, 116, 8, 1838-1856.
25. Witte, F.C. and Feenstra, P.H. (1998) “DIANA – Finite Element Analysis. User’s Manual: Release 7.2,” TNO Building Construction and Research, Delft, The Netherlands.